A drought stress-responsive metabolite malate modulates stomatal responses through G-protein-dependent pathway

Yoshiharu Mimata[1], Ruhai Gong[1,2], Xuanxuan Pei[1], Guochen Qin[1], Wenxiu Ye[1*]

[1]Peking University Institute of Advanced Agricultural Sciences, Weifang 261325, Shandong, China

[2]College of Horticulture, Shanxi Agricultural University, Taigu 030801, Shanxi, China

*Corresponding author: wenxiu.ye@pku-iaas.edu.cn

Running title: TCA cycle metabolites regulate guard cell signaling

Abstract

Drought poses a significant environmental threat to global agricultural production and distribution. Plant adaptation to dehydration stress involves intricate biological processes with substantial changes in metabolite composition. In this study, we investigated the role of tricarboxylic acid (TCA) cycle metabolites in drought tolerance in grapevine and Arabidopsis. Metabolome analysis revealed that malate, citrate, and isocitrate were upregulated over time in detached grapevine leaves. Five out of 10 organic acids tested, including TCA cycle metabolites, elicited increases in cytosolic free Ca^{2+} concentration ($[Ca^{2+}]_{cyt}$) in guard cells. Eight out of 10 directly activated a major anion channel in guard cell SLAC1, suggesting that SLAC1 is a general sensor of carboxylic acids. Furthermore, malate alone remarkably induced stomatal closure, which required increases in $[Ca^{2+}]_{cyt}$ in guard cells and activation of SLAC1. Pharmacological experiments suggested that cyclic ADP-ribose (cADPR), cAMP and inositol trisphosphate (IP_3) act as second messengers essential for malate-induced $[Ca^{2+}]_{cyt}$ elevation and stomatal closure. G-proteins, which regulate second messenger production, were identified as components of malate signaling. These results indicate that malate plays a key role in connecting metabolic regulation and drought tolerance. As TCA cycle intermediates are key players in stress responses in mammals as well, we propose that they are common stress-responsive signal molecules mediated by G-protein-dependent signal cascades in both the animal and plant kingdoms.

Introduction

Drought constitutes a major environmental stress with global implications for crop survival and yields. Grapevine (*Vitis*) is one of the oldest domesticated crops and holds crucial economic importance for industries through the production of wine, brandy, juice, table grapes, and raisins. Despite the increasing demand for grapes and grape products, the global vineyard area is diminishing annually. In 2023, wine production was anticipated to reach its lowest levels in 60 years, primarily due to the impacts of global climate change, especially drought conditions (http://www.oiv.int/). In response to drought, plants synthesize a phytohormone abscisic acid (ABA) and close stomatal pores, formed by pairs of guard cells in the epidermis of leaves, to prevent excessive water loss through guard cell signaling (Murata et al., 2015). Thus, gaining a comprehensive understanding of the molecular mechanisms underlying stomatal closure is crucial for enhancing drought tolerance in plants.

Stomatal closure is initiated by the transport of anions across the plasma membrane of guard cells through the slow-type anion channel encoded by the *SLOW ANION CHANNEL-ASSOCIATED 1* (*SLAC1*) gene (Schroeder et al., 2001; Negi et al., 2008; Vahisalu et al., 2008). SLAC1 is phosphorylated and activated by cytosolic Ca^{2+} sensor kinases, CALCIUM-DEPENDENT PROTEIN KINASEs (CDPKs) (Brandt et al., 2015), leading to a decrease in turgor pressure and subsequent stomatal closure. Cytosolic free Ca^{2+} acts as a ubiquitous second messenger, and its concentration transiently increases in response to environmental, developmental, and growth signals (Luan and Wang, 2021). The increase in cytosolic free Ca^{2+} concentration ($[Ca^{2+}]_{cyt}$) results from the uptake of Ca^{2+} into the cell and the release of Ca^{2+} from internal stores through Ca^{2+} channels in response to a membrane potential shift (Hamilton et al., 2000) and second messengers such as cyclic adenosine diphosphate ribose (cADPR) (Leckie et al., 1998), cyclic adenosine monophosphate (cAMP) (Lemtiri-Chlieh and Berkowitz, 2004), inositol trisphosphate (IP_3) (Gilroy et al., 1990), reactive oxygen species (ROS) (Pei et al., 2000), nitric oxide (NO) (Garcia-Mata et al., 2003), cyclic guanosine monophosphate (cGMP) (Wang et al., 2013), and nicotinic acid adenine dinucleotide phosphate (NAADP) (Navazio et al., 2000). In guard cells, cytosolic Ca^{2+} binds to the EF hands of CDPKs, leading to activation of CDPKs, which then induces stomatal closure through the phosphorylation of

63 SLAC1 (Brandt et al., 2015).

64 Heterotrimeric G-proteins, composed of Gα, Gβ, and Gγ subunits, play pivotal roles in the
65 generation of second messengers, thereby participating in various biological processes such as
66 growth, development, and responses to environmental stimuli (Jin et al., 2013; Pandey 2020).
67 The genome of *A. thaliana* encodes one canonical Gα (GPA1), one Gβ (AGB1), and three Gγ
68 subunits (AGG1–AGG3). GPA1 and/or AGB1 are involved in regulating stomatal movements
69 and activating slow-type anion channels (Wang et al., 2001; Fan et al., 2008; Yu et al., 2018).

70 The regulation of metabolism stands out as a key mechanism for maintaining cell osmotic
71 potential during abiotic stress. Despite a comprehensive description of metabolic responses to
72 dehydration stress in *Arabidopsis thaliana* (Urano et al., 2009), the specific contributions of
73 these metabolites to stress tolerance remain unclear. The metabolic reprogramming triggered
74 by drought leads to elevated tricarboxylic acid (TCA) cycle intermediates in Arabidopsis leaves
75 (Pires et al., 2016). TCA cycle intermediates play an essential role in providing energy fuels
76 and metabolic precursors. Recent findings have demonstrated that TCA cycle intermediates also
77 function as signaling molecules in mammals. Succinate modulates systemic energy metabolism
78 as a metabolic signal "metabokine" *via* G-protein signaling cascades (Krzak et al., 2021).
79 Malate as well as succinate directly binds to a G-protein coupled receptor and causes rapid
80 increases in intracellular [Ca^{2+}] and IP_3 accumulation (Trauelsen et al., 2017). In plants, malate
81 is crucial due to its significant associations with stomatal movements, aluminum toxicity, CO_2
82 fixation, ripening, and the taste of berries. Particularly in grapevines, malate is instrumental in
83 determining wine quality and facilitating the growth of microorganisms for vinification
84 (Sweetman et al., 2009; Fernie and Martinoia, 2009). The accumulation of malate is induced
85 by environmental changes and may be linked to physiological responses in various tissues such
86 as leaves, xylem, roots, and mesocarp (Van Kirk and Raschke, 1978; Kondo and Maruta, 1987;
87 Hedrich et al., 1994; Gabriel and Kesselmeier, 1999; Patonnier et al., 1999; Malcheska et al.,
88 2017; Delhaize et al., 1993; Wada et al., 2008). However, the regulatory mechanism of
89 physiological responses by TCA cycle metabolites remains unclear in plants.

90 Previous studies have shown that malate increases $[Ca^{2+}]_{cyt}$ and ROS production in guard cells

91 and directly activates SLAC1, leading to stomatal closure in *A. thaliana* (Mimata et al., 2022a;
92 2022b). In this study, we demonstrate that several TCA cycle metabolites accumulate in
93 grapevine leaves during dehydration stress, among which malate most effectively regulates
94 stomatal response *via* a G-protein signaling cascade. We propose that malate forms a hub
95 between energy homeostasis and stress response.

96

97 **Results**

98 **Metabolic responses of TCA cycle metabolites to dehydration stress in grapevine leaves**

99 To investigate metabolic changes in response to drought, grapevine (*Vitis vinifera*) leaves were
100 subjected to water-deficit stress. Detached leaves were sampled at 0–24 h of the dehydration
101 stress treatment and subjected to non-targeted metabolome analysis. Principal component
102 analysis (PCA) revealed that metabolite level changes were not pronounced between 0 and 1 h
103 but gradually increased thereafter (Figure 1A). Significant metabolite changes were classified
104 into three patterns: gradual decrease (subclass 1), gradual increase (subclass 2), and increase
105 followed by decrease (subclass 3) (Supplemental Figure 1A). The endogenous level of ABA,
106 an indicator of drought stress, increased after 2 h of dehydration stress and reached a plateau
107 after 6 h (Figure 1B). After 24 h of treatment, out of 2,407 metabolites, 436 were upregulated,
108 and 80 were downregulated (Figure 1C and Supplemental Data 1). Amino acids, lipids,
109 terpenoids, phenolic acids, alkaloids, and flavonoids were the primary categories exhibiting
110 changes (Figure 1D and Supplemental Figure 1B). Among the upregulated metabolites, we
111 specifically examined three TCA cycle metabolites—malate, isocitrate, and citrate—since
112 malate functions as a signaling molecule inducing stomatal closure (Mimata et al., 2022a).
113 Malate, isocitrate, and citrate increased after 12 or 24 h of dehydration stress (Figure 1E). In
114 contrast, *cis*-aconitate decreased immediately after 2–4 h and then returned to basal values.

115 **Effects of TCA cycle metabolites on the $[Ca^{2+}]_{cyt}$ in guard cells**

116 Since Ca^{2+} is a critical second messenger in guard cell signaling, we investigated the effects of
117 TCA cycle metabolites on the elevations of $[Ca^{2+}]_{cyt}$ through live cell imaging of *A. thaliana*

118 guard cells expressing a Ca^{2+} sensor fluorescent protein Yellow Cameleon 3.6. Exogenous
119 application of fumarate, malate, α-ketoglutarate, pyruvate, and acetate induced elevations in
120 $[Ca^{2+}]_{cyt}$, significantly increasing the frequency of $[Ca^{2+}]_{cyt}$ elevation (Figure 2 and
121 Supplementary Figure 2A). The malate-induced $[Ca^{2+}]_{cyt}$ increases were not observed in the
122 presence of a Ca^{2+} channel blocker La^{3+} (Figure 2A and 2D). These findings suggest that α-
123 hydroxy or α-keto acids (Supplementary Figure 2B) showed specificity in inducing $[Ca^{2+}]_{cyt}$
124 elevation in guard cells.

125 Interestingly, acetate caused transient long-term $[Ca^{2+}]_{cyt}$ increase (Figure 2A), likely due to its
126 higher pKa, leading to cytosolic acidification (Felle 1988), H^+-induced Ca^{2+} release from the
127 ER (Huang et al., 2023), and fluorescence quenching (Supplemental Figure 2A; Nagai et al.,
128 2004).

129 **Effects of TCA cycle metabolites on the activation of SLAC1 expressed in Xenopus oocytes**

130 Activation of the SLAC1 anion channel is crucial for stomatal closure (Vahisalu et al., 2008;
131 Negi et al., 2008). To explore the modulation of VvSLAC1 activity by TCA cycle metabolites,
132 we used a two-electrode voltage-clamp technique on Xenopus oocytes expressing VvSLAC1.
133 The negative currents in oocytes expressing VvSLAC1 were minimal (Supplementary Figure
134 3), resembling the characteristics of the inactive form of AtSLAC1 (Mimata et al., 2022a).
135 Constitutively active AtSLAC1 mutants, such as AtSLAC1T513D and AtSLAC1F450A,
136 exhibit substantial basal activity and their activity were further enhanced by malate in oocytes
137 (Chen et al., 2010; Maierhofer et al., 2014; Mimata et al., 2022a). Therefore, we expressed
138 VvSLAC1T503D, corresponding to AtSLAC1T513D, and VvSLAC1F440A, corresponding to
139 AtSLAC1F450A, in oocytes. These mutants exhibited 3.5- and 4.8-fold larger currents at −160
140 mV compared to oocytes expressing wild-type VvSLAC1, respectively (Supplementary Figure
141 3). We then analyzed VvSLAC1 activity during perfusion with bathing solution supplemented
142 with TCA cycle metabolites. Carboxylic acids did not increase the negative currents in oocytes
143 expressing wild-type VvSLAC1 (Figure 3A and 3C). On the other hand, all the carboxylic acids
144 except for acetate and pyruvate significantly increased the negative currents in oocytes
145 expressing VvSLAC1F440A (Figure 3A and 3C), similar to the results observed for AtSLAC1

146 (Figure 3B and 3D). Given the conservation of SLAC1 across various plant species (Hedrich
147 and Geiger, 2017), these findings suggest that SLAC1 may serve as a universal sensor for
148 carboxylic acids.

149 **Malate emerges as a specific modulator in the regulation of stomatal responses**

150 To assess how TCA cycle metabolites influence plant responses to drought stress, we measured
151 stomatal aperture in the presence of carboxylic acids. After stomata were fully open under light,
152 each carboxylic acid was applied, and stomatal aperture was measured. A significant reduction
153 in stomatal aperture was observed exclusively with malate treatment in *V. vinifera* (Figure 4A).
154 Consistent results were obtained using *A. thaliana* (Figure 4B). Furthermore, the malate-
155 induced stomatal closure was also observed in tomatoes and chili peppers (Supplemental Figure
156 4). These findings suggest that malate specifically acts as a modulator of stomatal closure, and
157 malate signaling is conserved across various plant species.

158 To further investigate the malate signaling pathway, we conducted a series of pharmacological
159 experiments (Supplemental Table 1). Malate-induced stomatal closure in both *V. vinifera* and *A.*
160 *thaliana* was abolished by anion channel blockers, 4,4′-diisothiocyano-2,2′-stilbenedisulfonic
161 acid (DIDS) and 9-anthracenecarboxylic acid (9-AC), an extracellular Ca^{2+} chelator 1,2-bis(2-
162 aminophenoxy)ethane-*N*,*N*,*N*′,*N*′-tetraacetic acid (BAPTA), and Ca^{2+} channel blockers,
163 nifedipine and La^{3+} (Figure 4C–4F; Mimata et al., 2022a). These results suggest anion channels
164 and Ca^{2+} signaling are essential for malate-induced stomatal closure in *V. vinifera* and *A.*
165 *thaliana*, consistent with the results for $[Ca^{2+}]_{cyt}$ and SLAC1 activity (Figure 2A, 2D and 3).

166 **Malate stimulates Ca^{2+} signaling *via* second messengers including cADPR, cAMP, and IP_3**

167 To further elucidate the malate-induced stomatal closure, the role of second messengers relevant
168 to Ca^{2+} signaling, including cADPR, cAMP, IP_3, ROS, NO, cGMP, NAADP, and PIP_3 (see
169 Introduction), was investigated by pharmacological approach. Nicotinamide, alloxan,
170 neomycin, and salicylhydroxamic acid (SHAM), which are inhibitors of cADPR, cAMP, IP_3
171 and peroxidase-catalyzed ROS production, respectively, completely abolished the malate-
172 induced stomatal closure in *V. vinifera* and *A. thaliana* (Figure 4C, 4D, 4F and 5A–C; Mimata

173 et al., 2022b). On the other hand, *N*-nitro-L-arginine methyl ester (L-NAME), 2-(4-
174 carboxyphenyl)-4,4,5,5-tetramethylimidazoline-1-oxyl-3-oxide (cPTIO), LY83583, Ned 19,
175 and wortmannin, which are an NO synthetase inhibitor, an NO scavenger, a guanylate cyclase
176 inhibitor, an antagonist of NAADP, and an inhibitor of PIP_3 production, respectively, have little
177 inhibitory effect on malate-induced stomatal closure (Supplementary Figure 5). Ca^{2+} imaging
178 experiments further showed that nicotinamide, alloxan, and neomycin but not SHAM inhibited
179 malate-induced $[Ca^{2+}]_{cyt}$ oscillations in Arabidopsis (Figure 5D and 5E). These results suggest
180 that Ca^{2+} signaling mediated by cADPR, cAMP, and IP_3 is required for malate-induced stomatal
181 closure.

182 **G-proteins are master regulators in malate signaling**

183 Since the generation of cADPR, cAMP, IP_3, and ROS is regulated by G-proteins (Zhang et al.,
184 2011; Jin et al., 2013), their roles in the stomatal response to malate were investigated with Gα
185 inhibitors YM-254890 and suramin, and Gβγ inhibitors gallein, guanosine 5′-*O*-(2-
186 thiodiphosphate) (GDPβS), and GRK2i. While YM-254890 did not suppress the malate-
187 induced stomatal closure, all other inhibitors completely abolished the malate effect in *V.*
188 *vinifera* and *A. thaliana* (Supplemental Figure 5E and 5F; Figure 6A and 6B). Furthermore,
189 stomata of *gpa1* and *agb1*, loss-of-function mutants of Arabidopsis canonical Gα subunit and
190 Gβ subunit, were insensitive to malate (Figure 6C). GDPβS also completely suppressed malate-
191 induced ROS production (Figure 6D). These data together suggest that malate signal is
192 transduced by G-proteins in guard cells.

193

194 **Discussion**

195 Drought has severe impacts on agricultural crops and results in metabolite fluctuations in plants.
196 In this study, we identified 436 upregulated and 80 downregulated metabolites in grapevine
197 leaves in response to dehydration stress (Figure 1C). These included modulators of stomatal
198 movements, such as ABA, phaseic acid, indole-3-acetic acid, jasmonic acid, 5-aminolevulinic
199 acid, γ-aminobutyric acid, adenosine-3'-5'-diphosphate, malic acid, spermidine, resveratrol,

200 cinnamic acid, gallic acid, and ascorbic acid (Supplemental Data 1). This study specifically
201 focused on the effect of the primary metabolite and clarified the mechanism underlying stomatal
202 closure triggered by a major TCA cycle metabolite malate.

203 **Specific guard cell responses triggered by TCA cycle metabolites**

204 TCA cycle metabolites, as carboxylic acids, elicit distinct guard cell responses, including
205 increases in $[Ca^{2+}]_{cyt}$, activation of SLAC1, and stomatal closure (Figure 2–4). The limited
206 specificity of the Ca^{2+} response to TCA cycle metabolites (Figure 2), compared to SLAC1
207 activation (Figure 3), suggests that SLAC1 activation does not necessarily lead to increases in
208 $[Ca^{2+}]_{cyt}$, and a carboxylate receptor independent from SLAC1 may exist. Despite both α-
209 ketoglutarate and oxaloacetate are α-keto acids, only α-ketoglutarate, with a carbon chain length
210 similar to glutamate, was effective in inducing elevation of $[Ca^{2+}]_{cyt}$ (Figure 2A and 2D),
211 indicating the importance of carbon chain length in perception. Dicarboxylate glutamate
212 induces $[Ca^{2+}]_{cyt}$ elevation in guard cells through a pathway dependent on glutamate receptor-
213 like channels (GLRs), while malate signaling is independently of GLRs (Mimata et al., 2022a).
214 Therefore, it is plausible that α-ketoglutarate is recognized by GLRs.

215 Although fumarate and α-ketoglutarate caused Ca^{2+} elevation and SLAC1 activation (Figure
216 2A, 2D and 3), they failed to close the stomata (Figure 4A and 4B), suggesting that Ca^{2+}
217 elevation and SLAC1 activation alone are insufficient for stomatal closure. It remains unclear
218 why only malate induce stomatal closure. Additionally, we observed enhanced ROS production
219 with fumarate and α-ketoglutarate, similar to malate (Supplemental Figure 6A). Therefore,
220 unknown factors specific to malate, rather than fumarate and α-ketoglutarate, require further
221 elucidation in future studies.

222 **Malate plays a key role in stress responses**

223 In a related study, the relative abundance of malate increased 6.78-fold in Arabidopsis aerial
224 parts after 10 hours of dehydration stress (Urano et al., 2009). Malate was observed to be
225 secreted during stomatal closure (Van Kirk and Raschke, 1978), with its content in guard cells
226 decreasing after ABA treatment (Kondo and Maruta, 1987; Jin et al., 2013). Notably, the malate

227 exporter AtALMT12, mainly expressed in guard cells and localized at the plasma membrane,
228 is activated through the ABA signaling pathway (Sasaki et al., 2010; Meyer et al., 2010), and
229 loss-of-function mutation of AtALMT12 have been shown to increase malate content in leaves
230 and result in malate insensitivity (Medeiros et al., 2016; Sasaki et al., 2022). These findings
231 suggest that malate accumulates in leaves under water deficit conditions and is secreted into the
232 apoplast in response to ABA. Malate was the most potent TCA cycle metabolites which
233 modulates stomatal aperture (Figure 4A and 4B). Feeding malate through the petiole decreases
234 stomatal aperture and stomatal conductance (Patonnier et al., 1999; Malcheska et al., 2017;
235 Rasulov et al., 2018). Therefore, its accumulation under dry conditions induces stomatal closure,
236 minimizing water loss and facilitating adaptation to desiccation. Malate is not only closely
237 related to drought stress but is also implicated in stomatal immunity. Some carboxylic acids
238 associated with the TCA cycle, including malate, are detected in the apoplastic fluid from cells
239 treated with an elicitor just before apoplastic oxidative burst (Bolwell et al., 2002). Blockers of
240 malate-permeable channels repress antibacterial ROS production and pathogen resistance
241 (Colcombet et al., 2009). Indeed, malate induced ROS production (Figure 6D; Mimata et al.,
242 2022b). These findings highlight malate as a promising candidate for controlling disease
243 resistance in plants.

244 **Malate signaling is mediated by a specific set of second messengers**

245 Stomatal measurements and Ca^{2+} imaging using inhibitors suggest the involvement of second
246 messengers cADPR, cAMP, and IP_3 in malate signaling (Figure 4C, 4D, 4F, 5A, 5D and 5E).
247 Malate-induced stomatal closure was also impaired by the inhibitor of peroxidase (Figure 5B
248 and 5C). Malate promotes ROS production by peroxidases (Mimata et al., 2022b), and ROS
249 activate plasma membrane Ca^{2+} channels and increase $[Ca^{2+}]_{cyt}$ (Pei et al., 2000) in *A. thaliana*.
250 Thus, we hypothesized that malate accelerates Ca^{2+} influx by promoting ROS production.
251 Contrary to our expectation, the inhibition of ROS production did not impair malate-induced
252 Ca^{2+} responses (Figure 5D and 5E). Moreover, blocking Ca^{2+} influx did not affect ROS
253 production (Supplemental Figure 6B), indicating that ROS production is independent of Ca^{2+}
254 signaling in malate-induced stomatal closure.

255 **Malate signaling is transduced by G-protein signaling cascades**

256 Pharmacological and reverse genetics experiments suggest that G-proteins are master regulators
257 in malate signaling (Figure 6). Based on the current results, we propose a model to summarize
258 malate signaling in guard cells (Figure 6E). The external signal of malate is transmitted by G-
259 proteins, which modulate the generation of second messengers, including cAMP, cADPR and
260 IP_3. This cascade leads to increases in $[Ca^{2+}]_{cyt}$, resulting in the phosphorylation of SLAC1 by
261 CDPKs. Additionally, G-proteins simultaneously modulate ROS production, which contributes
262 to SLAC1 phosphorylation. Extracellular malate directly promotes anion transport through
263 phosphorylated SLAC1, leading to a decrease in turgor pressure and subsequent stomatal
264 closure.

265 In mammals, carboxylates are sensed by G-protein-coupled receptors (GPCRs). Succinate is
266 released into the extracellular space from stimulated macrophages and injured tissues, with
267 local concentrations reaching millimolar levels (Chouchani et al, 2014; Littlewood-Evans et al.,
268 2016). Extracellular succinate activates GPCRs, stimulating IP_3 formation, inhibiting cAMP
269 production, and increasing $[Ca^{2+}]_{cyt}$ *via* the G-protein signaling pathway (He et al., 2004;
270 Trauelsen et al., 2021). Similarly, malate is perceived by the succinate receptor and causes rapid
271 increases in intracellular $[Ca^{2+}]$ and IP_3 accumulation (Trauelsen et al., 2017). Since plant
272 GPCRs differ significantly from those in animals, and GPCRs with guanine nucleotide
273 exchange factor activity have not yet been identified, it is challenging to identify malate
274 receptors. Nevertheless, based on the shared signaling components, we propose that TCA cycle
275 metabolites are common stress-responsive signal molecules mediated by G-protein-dependent
276 signaling cascades in both animal and plant kingdoms.

277

278 **Materials and methods**

279 **Plants and growth conditions**

280 Grapevine (*V. vinifera* L. cv. Chardonnay) was grown on a soil mixture of 1:1 = soil: vermiculite
281 (v/v) in a growth room at 24 °C and 80% relative humidity under 16 h-light/8 h-dark

282 photoperiod with a photon flux density of 100 μmol m^{-2} s^{-1}. Arabidopsis (*A. thaliana* L. ecotype
283 Colombia-0) was grown on a soil mixture of 1:1 = soil: vermiculite (v/v) in a growth chamber
284 at 21 °C and 60% relative humidity under 16 h-light/8 h-dark photoperiod with a photon flux
285 density of 120 μmol m^{-2} s^{-1}. The T-DNA insertion lines, *gpa1-4* (SALK_001846) and *agb1*
286 (SALK_077086C), were obtained from Arashare (https://www.arashare.cn/index/).

287 Tomato (*Solanum lycopersicum* L. cv. Micro-Tom) was used. Tomato was grown on a soil
288 mixture of 1:1 = soil: vermiculite (v/v) in a glass greenhouse at 15 °C and 60% relative humidity.
289 Chili pepper (*Capsicum chinense* L. cv. Trinidad Moruga scorpion) was used. Chili pepper was
290 grown on a soil mixture of 1:1 = soil: vermiculite (v/v) in a glass greenhouse at 22 °C and 50%
291 relative humidity.

292 **Dehydration stress treatment**

293 Fully expanded leaves from 1 to 2-month-old grapevine plants were randomly detached.
294 Dehydration was performed as described previously (Urano et al., 2009) with a few
295 modifications. The detached leaves were exposed to dehydration stress on the paper at 26℃
296 and ambient humidity under light. At indicated time, the leaves were frozen by liquid nitrogen.

297 **Sample preparation for LC-MS**

298 The sample preparation, extract analysis, metabolite identification and quantification were
299 performed at Wuhan MetWare Biotechnology Co., Ltd (www.metware.cn) following their
300 standard procedures. The samples were freeze-dried in a lyophilizer (Scientz-100F; Scientz,
301 Zhejiang, China) and then homogenized (30 Hz, 1.5 min) into powder using a grinder (MM
302 400; Retsch, Dusseldorf, Germany). Next, 1200 μL of -20 °C pre-cooled 70% methanolic
303 aqueous internal standard extract added to 50 mg of sample powder. The sample was vortexed
304 once every 30 min for 30 s, for a total of 6 times. After centrifugation at 12000rpm for 3min,
305 the supernatant was aspirated, and the sample was filtered through a microporous membrane
306 (0.22 μm pore size) and stored in the injection vial for UPLC-MS/MS analysis.

307 **Metabolite analysis using LC-MS**

308 The sample extracts were analyzed using an UPLC-ESI-MS/MS system (UPLC, ExionLC™
309 AD: SCIEX, MA, USA; MS, Applied Biosystems 4500 Q TRAP: SCIEX). The analytical
310 conditions were as follows, UPLC: column, Agilent SB-C18 (1.8 μm, 2.1 mm * 100 mm); The
311 mobile phase was consisted of solvent A, pure water with 0.1% formic acid, and solvent B,
312 acetonitrile with 0.1% formic acid. Sample measurements were performed with a gradient
313 program that employed the starting conditions of 95% A, 5% B. Within 9 min, a linear gradient
314 to 5% A, 95% B was programmed, and a composition of 5% A, 95% B was kept for 1 min.
315 Subsequently, a composition of 95% A, 5.0% B was adjusted within 1.1 min and kept for 2.9
316 min. The flow velocity was set as 0.35 mL per minute; The column oven was set to 40°C; The
317 injection volume was 4 μL. The effluent was alternatively connected to an ESI-triple
318 quadrupole-linear ion trap (QTRAP)-MS.

319 The ESI source operation parameters were as follows: source temperature 550°C; ion spray
320 voltage (IS) 5500 V (positive ion mode)/-4500 V (negative ion mode); ion source gas I (GSI),
321 gas II (GSII), curtain gas (CUR) were set at 50, 60, and 25 psi, respectively; the collision-
322 activated dissociation (CAD) was high. QQQ scans were acquired as MRM experiments with
323 collision gas (nitrogen) set to medium. DP (declustering potential) and CE (collision energy)
324 for individual MRM transitions was done with further DP and CE optimization. A specific set
325 of MRM transitions were monitored for each period according to the metabolites eluted within
326 this period.

327 **Sample preparation for GC-MS**

328 The leaves subjected dehydration stress were ground to a powder in liquid nitrogen. 500 mg (1
329 mL) of the powder was transferred immediately to a 20 mL head-space vial (Agilent, CA, USA),
330 containing NaCl saturated solution, to inhibit any enzyme reaction. The vials were sealed using
331 crimp-top caps with TFE-silicone headspace septa (Agilent). At the time of SPME analysis,
332 each vial was placed in 60 °C for 5 min, then a 120 μm DVB/CWR/PDMS fiber (Agilent) was
333 exposed to the headspace of the sample for 15 min at 60 °C.

334 **Metabolite analysis using GC-MS**

335 After sampling, desorption of the VOCs from the fiber coating was carried out in the injection
336 port of the GC apparatus (Model 8890; Agilent) at 250°C for 5 min in the splitless mode. The
337 identification and quantification of VOCs was carried out using an Agilent Model 8890 GC and
338 a 7000D mass spectrometer (Agilent), equipped with a 30 m × 0.25 mm × 0.25 μm DB-5MS
339 (5% phenyl-polymethylsiloxane) capillary column. Helium was used as the carrier gas at a
340 linear velocity of 1.2 mL/min. The injector temperature was kept at 250°C and the detector at
341 280°C. The oven temperature was programmed from 40°C (3.5 min), increasing at 10°C/min
342 to 100°C, at 7°C/min to 180°C, at 25°C/min to 280°C, hold for 5 min. Mass spectra was
343 recorded in electron impact (EI) ionization mode at 70 eV. The quadrupole mass detector, ion
344 source and transfer line temperatures were set, respectively, at 150, 230 and 280°C. The MS
345 was selected ion monitoring (SIM) mode was used for the identification and quantification of
346 analytes.

347 **Data analysis of the non-target metabolome**

348 Relative metabolite abundances were calculated by the peak areas. Unsupervised PCA was
349 performed by statistics function prcomp within R (www.r-project.org). The relative contents of
350 all differential metabolites were processed by UV (unit variance scaling) followed by K-Means
351 cluster analysis. Identified metabolites were annotated using KEGG Compound database
352 (http://www.kegg.jp/kegg/compound/). Pathways with significantly regulated metabolites
353 mapped to were then fed into metabolite sets enrichment analysis (MSEA), their significance
354 was determined by hypergeometric test's p-values. Upregulated metabolites are defined VIP >
355 1, $\log_2$ (Fold change) ≥ 1 and P-value > 0.05, downregulated metabolites are defined VIP > 1,
356 $\log_2$ (Fold change) ≤ −1 and P-value > 0.05. P-value was calculated by Welch's t-test.

357 **$[Ca^{2+}]_{cyt}$ imaging**

358 Wild-type Arabidopsis plants expressing Yellow Cameleon 3.6 were used to measure $[Ca^{2+}]_{cyt}$
359 in guard cells as described previously (Mimata et al., 2022a). The abaxial side of an excised
360 rosette leaf was gently attached to a glass slide with a medical adhesive (stock no. 7730;
361 Hollister, IL, USA) and then mesophyll tissues were whittled away with a razor blade to keep
362 the abaxial epidermis intact on the slide. The remaining abaxial epidermis was immersed in

363 stomatal assay solution, comprising 5 mM KCl, 50 μM $CaCl_2$ and 10 mM MES/Tris (pH 5.6),
364 in the light for 2 h to induce stomatal opening. The epidermis was treated with 10 mM organic
365 acid in stomatal assay solution at 3 min after monitoring and with 10 mM $CaCl_2$ at 18 or 28 min
366 after the measurement to check responsiveness. Inhibitors were added 5 min before starting
367 imaging. The stock solution of organic acids was dissolved in stomatal assay solution and
368 adjusted to a pH of 5.6 with Tris.

369 The images were acquired under a fluorescence microscope (ECLIPSE Ti2-E; NIKON).
370 Excitation light was provided by a mercury arc lamp and a 436 nm filter (ET436/20x, Chroma
371 Technology Corporation, VT, USA). Emission of the CFP was measured at 480 nm filter
372 (ET480/40m, Chroma Technology Corporation) and of the YFP at 535 nm filter (ET535/30m,
373 Chroma Technology Corporation) using a CMOS camera (ORCA-Fusion BT Digital CMOS
374 camera C15440; HAMAMATSU, Shizuoka, Japan). Images were taken every 5 s.

375 **Cloning and cRNA synthesis**

376 All constructs were cloned into the oocyte expression vector pNB1u (Nour-Eldin et al., 2006)
377 by ClonExpress II One Step Cloning Kit (Vazyme Biotech, Nanjing, China). The site-directed
378 mutants were generated by FastCloning (Li et al., 2011). VvSLAC1 (LOC100244459) cDNA
379 from *V. vinifera* was used for cloning, and all constructs were verified by sequencing. Primers
380 used for cloning and site-directed mutagenesis are listed in Supplemental Table 2. cRNA was
381 prepared using an mMESSAGE mMACHINE ™ T7 Transcription Kit (Thermo Fisher
382 Scientific, MA, USA).

383 **Two-electrode voltage-clamp**

384 *Xenopus laevis* oocytes were injected with 50 nL cRNA (each 10 ng) and incubated in ND96
385 buffer at 18°C for a few days before voltage-clamp recordings (Mimata et al., 2022a). The bath
386 solution contained 1 mM Mg-gluconate, 1 mM Ca-gluconate and 1 mM $LaCl_3$ ± 10 mM organic
387 acid buffered with 10 mM MES/Tris to adjust the pH to 5.6. Osmolality was adjusted to 220
388 mM using D-sorbitol. The voltage pulse was commanded to clamp the membrane potential from
389 +60 mV to −120 mV in ramp for 1.8 seconds or from +60 to −160 mV in 20 mV decrements in

390 step for 2.5 seconds with a holding potential of 0 mV. Voltage-clamp recordings for oocytes
391 were performed using an Axoclamp 900A amplifier (Molecular Devices, CA, USA), data were
392 acquired using a Digidata 1550B system (Molecular Devices) and analyzed using pCLAMP
393 11.2 software (Molecular Devices).

394 **Measurement of stomatal aperture**

395 Stomatal apertures were measured as described previously (Ye et al., 2020) with modifications.
396 Leaf discs (4 mm in diameter) obtained from fully expanded leaves were placed abaxial side
397 down on stomatal assay solution. The discs were exposed to light for 2 h to induce stomatal
398 opening and subsequently treated with 10 mM organic acid in stomatal assay solution for an
399 additional 2 h. Inhibitors were added 5 min before malate treatment. The abaxial epidermis was
400 captured under optical microscopes (ECLIPSE Ts-2R, ECLIPSE Ti2-E and ECLIPSE Ci;
401 NIKON, Tokyo, Japan) using NIS ELEMENTS software (NIKON). Stomatal apertures were
402 quantified using IMAGEJ software (NIH). We measured 30 stomatal apertures from a leaf disc
403 to calculate an average. This measurement was repeated four times using different plants, and
404 the overall average was calculated.

405 **Measurement of ROS production**

406 ROS production in guard cells was analyzed using the fluorescent dye 2',7'-
407 dihydrodichlorofluorescein diacetate (H_2DCF-DA) as described previously (Mimata et al.,
408 2022b) with modifications. The abaxial side of an excised rosette leaf was gently attached to a
409 glass slide with a medical adhesive and then mesophyll tissues were whittled away with a razor
410 blade. The remaining abaxial epidermis was immersed in stomatal assay solution in the light
411 for 2 h to induce stomatal opening. A total of 50 μM H_2DCF-DA was added to the stomatal
412 assay solution and the epidermal tissues were incubated in the dark for 30 min. After the dye
413 loading, the epidermal tissues were gently rinsed with stomatal assay solution. The epidermis
414 was treated with 10 mM organic acid ± inhibitor in stomatal assay solution. After the 30 min
415 incubation, fluorescent signals were captured using the fluorescence microscope with 480 ± 15
416 nm/ 535 ± 23 nm excitation/emission filters. We measured 30 guard cells from an epidermis to
417 calculate an average. This measurement was repeated three times using different plants, and the

418 overall average was calculated.

419 **Acknowledgements**

420 We thank Dr. Shangwei Zhong and Dr. Xu Wang (Peking University Institute of Advanced
421 Agricultural Sciences) for providing plant materials; Dr. Hussam Hassan Nour-Eldin
422 (University of Copenhagen) for providing pNB1u vector; Dr. Yoshiyuki Murata and Dr.
423 Shintaro Munemasa (Okamaya University) for providing Arabidopsis cDNA plasmid
424 constructs; Dongyue Wang (Peking University Institute of Advanced Agricultural Sciences) for
425 helping cloning. W.Y. laboratory is supported by Taishan Scholars Program of Shandong
426 Province and Shandong Provincial Science and Technology Innovation Fund.

427 **Conflict of interests**

428 The authors declare no competing interests.

429 **Contributions**

430 Y.M. and W.Y. designed the experiments. Y.M. analyzed all data and performed all experiments
431 except metabolomics. R.G. measured stomatal aperture and ROS production. X.P. conducted
432 metabolomics and G.Q. interpreted the data. Y.M. and W.Y. wrote the manuscript.

433 **Data availability**

434 The data underlying this article are available in the article and in its online supplementary
435 material.

436 **References**

437 Bolwell, G.P., Bindschedler, L.V., Blee, K.A., Butt, V.S., Davies, D.R., Gardner, S.L., Gerrish,
438 C., Minibayeva, F. (2002) The apoplastic oxidative burst in response to biotic stress in plants:
439 a three-component system. *J. Exp. Bot.* 10.1093/jexbot/53.372.1367.

440 Brandt, B., Munemasa, S., Wang, C., Nguyen, D., Yong, T., Yang, P.G., Poretsky, E., Belknap,
441 T.F., Waadt, R., Alemán F., et al. (2015) Calcium specificity signaling mechanisms in abscisic

442 acid signal transduction in Arabidopsis guard cells. *Elife* 10.7554/eLife.03599.

443 Chen, Y., Hu, L., Punta, M., Bruni, R., Hillerich, B., Kloss, B., Rost, B., Love, J., Siegelbaum,
444 S.A., Hendrickson, W.A. (2010) Homologue structure of the SLAC1 anion channel for closing
445 stomata in leaves. *Nature* 10.1038/nature09487.

446 Chouchani, E.T., Pell, V.R., Gaude, E., Aksentijević, D., Sundier, S.Y., Robb, E.L., Logan, A.,
447 Nadtochiy, S.M., Ord, E.N.J., Smith, A.C., et al. (2014) Ischaemic accumulation of succinate
448 controls reperfusion injury through mitochondrial ROS. *Nature* 10.1038/nature13909.

449 Colcombet, J., Mathieu, Y., Peyronnet, R., Agier, N., Lelièvre, F., Barbier-Brygoo, H., Frachisse,
450 J.-M. (2009) R-type anion channel activation is an essential step for ROS-dependent innate
451 immune response in *Arabidopsis* suspension cells. *Funct. Plant Biol.* 10.1071/FP09096.

452 Delhaize, E., Ryan, P.R., Randall, P.J. (1993) Aluminum Tolerance in Wheat (*Triticum aestivum*
453 L.) (II. Aluminum-Stimulated Excretion of Malic Acid from Root Apices). *Plant Physiol.*
454 10.1104/pp.103.3.695.

455 Fan, L.-M., Zhang, W., Chen, J.-G., Taylor, J.P., Jones, A.M., Assmann, S.M. (2008) Abscisic
456 acid regulation of guard-cell K^+ and anion channels in Gβ- and RGS-deficient *Arabidopsis* lines.
457 *Proc. Natl. Acad. Sci. USA.* 10.1073/pnas.0800980105.

458 Felle, H. (1988) Auxin causes oscillations of cytosolic free calcium and pH in *Zea mays*
459 coleoptiles. *Planta*. 10.1007/BF00634478.

460 Fernie, A.R., Martinoia, E. (2009) Malate. Jack of all trades or master of a few? *Phytochemistry*
461 10.1016/j.phytochem.2009.04.023.

462 Gabriel, R., Kesselmeier, J. (1999) Apoplastic solute concentrations of organic acids and
463 mineral nutrients in the leaves of several fagaceae. *Plant Cell Physiol.*
464 10.1093/oxfordjournals.pcp.a029583.

465 Garcia-Mata, C., Gay, R., Sokolovski, S., Hills, A., Lamattina, L., Blatt, M.R. (2003) Nitric
466 oxide regulates K^+ and Cl^- channels in guard cells through a subset of abscisic acid-evoked

467 signaling pathways. *Proc. Natl. Acad. Sci. USA.* 10.1073/pnas.1434381100.

468 Gilroy, S., Read, N.D., Trewavas, A.J. (1990) Elevation of cytoplasmic calcium by caged
469 calcium or caged inositol triphosphate initiates stomatal closure. *Nature* 10.1038/346769a0.

470 Hamilton, D.W.A., Hills, A., Köhler, B., Blatt, M.R. (2000) Ca^{2+} channels at the plasma
471 membrane of stomatal guard cells are activated by hyperpolarization and abscisic acid. *Proc.*
472 *Natl. Acad. Sci. USA.* 10.1073/pnas.080068897.

473 He, W., Miao, F.J.P., Lin, D.C.H., Schwandner, R.T., Wang, Z., Gao, J., Chen, J.-L., Tian, H.,
474 Ling, L. (2004) Citric acid cycle intermediates as ligands for orphan G-protein-coupled
475 receptors. *Nature* 10.1038/nature02488.

476 Hedrich, R., Marten, I., Lohse, G., Dietrich, P., Winter, H., Lohaus, G., Heldt, H.-W. (1994)
477 Malate-sensitive anion channels enable guard cells to sense changes in the ambient CO_2
478 concentration. *Plant J.* 10.1046/j.1365-313X.1994.6050741.x.

479 Hedrich, R., Geiger, D. (2017) Biology of SLAC1-type anion channels – from nutrient uptake
480 to stomatal closure. *New Phytol.* 10.1111/nph.14685.

481 Huang, S., Shen, L., Roelfsema, M.R.G., Becker, D., Hedrich, R. (2023) Light-gated
482 channelrhodopsin sparks proton-induced calcium release in guard cells. *Science*
483 10.1126/science.adj9696.

484 Jin, X., Wang, R.-S., Zhu, M., Jeon, B.W., Albert, R., Chen, S., Assmann, S.M. (2013) Abscisic
485 acid-responsive guard cell metabolomes of *Arabidopsis* wild-type and *gpa1* G-protein mutants.
486 *Plant Cell* 10.1105/tpc.113.119800.

487 Kondo, N., Maruta, I. (1987) Abscisic acid-induced stomatal closure in *Vicia faba* epidermal
488 strip. Excretion of solutes from guard cells and increase in elastic modulus of guard cell wall.
489 *Plant Cell Physiol.* 10.1093/oxfordjournals.pcp.a077303.

490 Krzak, G., Willis, C.M., Smith, J.A., Pluchino, S., Peruzzotti-Jametti, L. (2021) Succinate
491 Receptor 1: An Emerging Regulator of Myeloid Cell Function in Inflammation. *Trends*

492 *Immunol.* 10.1016/j.it.2020.11.004.

493 Leckie, C.P.,McAinsh, M.R., Allen, G.J., Sanders, D., Hetherington, A.M. (1998) Abscisic acid-
494 induced stomatal closure mediated by cyclic ADP-ribose. *Proc. Natl. Acad. Sci. USA.*
495 10.1073/pnas.95.26.15837.

496 Lemtiri-Chlieh, F., Berkowitz, G.A. (2004) Cyclic adenosine monophosphate regulates calcium
497 channels in the plasma membrane of Arabidopsis leaf guard and mesophyll cells. *J. Biol. Chem.*
498 10.1074/jbc.M400311200.

499 Lepetit, M., Brouquisse, R. (2023) Control of the rhizobium–legume symbiosis by the plant
500 nitrogen demand is tightly integrated at the whole plant level and requires inter-organ systemic
501 signaling. *Front. Plant Sci*. 10.3389/fpls.2023.1114840.

502 Li, C., Wen, A., Shen, B., Lu, J., Huang, Y., Chang, Y. (2011) FastCloning: a highly simplified,
503 purification-free, sequence- and ligation-independent PCR cloning method. *BMC Biotechnol*.
504 10.1186/1472-6750-11-92.

505 Littlewood-Evans, A., Sarret, S., Apfel, V., Loesle, P., Dawson, J., Zhang, J., Muller, A., Tigani,
506 B., Kneuer, R., Patel, S., et al. (2016) GPR91 senses extracellular succinate released from
507 inflammatory macrophages and exacerbates rheumatoid arthritis. *J. Exp. Med.*
508 10.1084/jem.20160061.

509 Luan, S., Wang, C. (2021) Calcium Signaling Mechanisms Across Kingdoms. *Annu. Rev. Cell*
510 *Dev. Biol.* 10.1146/annurev-cellbio-120219-035210.

511 Malcheska, F., Ahmad, A., Batool, S., Müller, H.M., Ludwig-Müller, J., Kreuzwieser, J.,
512 Randewig, D., Hänsch, R., Mendel, R.R., Hell, R., et al. (2017) Drought-Enhanced Xylem Sap
513 Sulfate Closes Stomata by Affecting ALMT12 and Guard Cell ABA Synthesis. *Plant Physiol.*
514 10.1104/pp.16.01784.

515 Maierhofer, T., Diekmann, M., Offenborn, J.N., Lind, C., Bauer, H., Hashimoto, K., Al-Rasheid,
516 K.A.S., Luan, S., Kudla, J., Geiger, D., et al. (2014) Site- and kinase-specific phosphorylation-
517 mediated activation of SLAC1, a guard cell anion channel stimulated by abscisic acid. *Sci.*

Signal. 10.1126/scisignal.2005703.

Medeiros, D.B., Martins, S.C.V., Cavalcanti, J.H.F., Daloso, D.M., Martinoia, E., Nunes-Nesi, A., DaMatta, F.M., Fernie, A.R., Araújo, W.L. (2016) Enhanced Photosynthesis and Growth in *atquac1* Knockout Mutants Are Due to Altered Organic Acid Accumulation and an Increase in Both Stomatal and Mesophyll Conductance. *Plant Physiol.* 10.1104/pp.15.01053.

Medeiros, D.B., Barros, K.A., Barros, J.A.S., Omena-Garcia, R.P., Arrivault, S., Sanglard, L.M.V.P., Detmann, K.C., Silva, W.B., Daloso, D.M., DaMatta, F.M., et al. (2017) Impaired Malate and Fumarate Accumulation Due to the Mutation of the Tonoplast Dicarboxylate Transporter Has Little Effects on Stomatal Behavior. *Plant Physiol*. 10.1104/pp.17.00971.

Meyer, S., Mumm, P., Imes, D., Endler, A., Weder, B., Al-Rasheid, K.A.S., Geiger, D., Marten, I., Martinoia, E., Hedrich, R. (2010) *At*ALMT12 represents an R-type anion channel required for stomatal movement in Arabidopsis guard cells. *Plant J.* 10.1111/j.1365-313X.2010.04302.x.

Mimata, Y., Munemasa, S., Nakamura, T., Nakamura, Y., Murata, Y. (2022a) Extracellular malate induces stomatal closure via direct activation of guard-cell anion channel SLAC1 and stimulation of Ca^{2+} signalling. *New Phytol.* 10.1111/nph.18400.

Mimata, Y., Munemasa, S., Akter, F., Jahan, I., Nakamura, T., Nakamura, Y., Murata, Y. (2022b) Malate induces stomatal closure via a receptor-like kinase GHR1- and reactive oxygen species-dependent pathway in *Arabidopsis thaliana*. *Biosci. Biotechnol. Biochem*. 10.1093/bbb/zbac122.

Murata, Y., Mori, I.C., Munemasa, S. (2015) Diverse Stomatal Signaling and the Signal Integration Mechanism. *Annu. Rev. Plant Biol.* 10.1146/annurev-arplant-043014-114707.

Nagai, T., Yamada, S., Tominaga, T., Ichikawa, M., Miyawaki, A. (2004) Expanded dynamic range of fluorescent indicators for Ca^{2+} by circularly permuted yellow fluorescent proteins. *Proc. Natl. Acad. Sci. USA.* 10.1073/pnas.0400417101.

Navazio, L., Bewell, M.A., Siddiqua, A., Dickinson, G.D., Galione, A., Sanders, D. (2000) Calcium release from the endoplasmic reticulum of higher plants elicited by the NADP

544 metabolite nicotinic acid adenine dinucleotide phosphate. *Proc. Natl. Acad. Sci. USA.*
545 10.1073/pnas.140217897.

546 Negi, J., Matsuda, O., Nagasawa, T., Oba, Y., Takahashi, H., Kawai-Yamada, M., Uchimiya, H.,
547 Hashimoto, M., Iba, K. (2008) CO_2 regulator SLAC1 and its homologues are essential for anion
548 homeostasis in plant cells. *Nature* 10.1038/nature06720.

549 Neill, S., Barros, R., Bright, J., Desikan, R., Hancock, J., Harrison, J., Morris, P., Ribeiro, D.,
550 Wilson, I. (2008) Nitric oxide, stomatal closure, and abiotic stress. *J. Exp. Bot.*
551 10.1093/jxb/erm293.

552 Nour-Eldin, H.H., Hansen, B.G., Nørholm, M.H.H., Jensen, J.K., Halkier, B.A. (2006)
553 Advancing uracil-excision based cloning towards an ideal technique for cloning PCR fragments.
554 *Nucleic Acids Res*. 10.1093/nar/gkl635.

555 Pandey S. (2020) Plant receptor-like kinase signaling through heterotrimeric G-proteins. *J. Exp.*
556 *Bot.* 10.1093/jxb/eraa016.

557 Patonnier, M.P., Peltier, J.P., Marigo, G. (1999) Drought-induced increase in xylem malate and
558 mannitol concentrations and closure of *Fraxinus excelsior* L. stomata. *J. Exp. Bot.*
559 10.1093/jxb/50.336.1223.

560 Pei, Z.M., Murata, Y., Benning, G., Thomine, S., Klüsener, B., Allen, G.J., Grill, E., Schroeder,
561 J.I. (2000) Calcium channels activated by hydrogen peroxide mediate abscisic acid signalling
562 in guard cells. *Nature* 10.1038/35021067.

563 Pires, M.V., Júnior, A.A.P., Medeiros, D.B., Daloso, D.M., Pham, P.A., Barros, K.A., Engqvist,
564 M.K.M., Florian, A., Krahnert, I., Maurino, V.G., et al. (2016) The influence of alternative
565 pathways of respiration that utilize branched-chain amino acids following water shortage in
566 *Arabidopsis*. *Plant Cell Environ.* 10.1111/pce.12682.

567 Prokic, L., Jovanovic, Z., McAinsh, M.R., Vucinic, Z., Stikic, R. (2006) Species-dependent
568 changes in stomatal sensitivity to abscisic acid mediated by external pH. *J. Exp. Bot.*
569 10.1093/jxb/erj057.

570 Rasulov, B., Talts, E., Bichele, I., Niinemets, Ü. (2018) Evidence That Isoprene Emission Is
571 Not Limited by Cytosolic Metabolites. Exogenous Malate Does Not Invert the Reverse
572 Sensitivity of Isoprene Emission to High [CO_2]. *Plant Physiol.* 10.1104/pp.17.01463.

573 Sasaki, T., Mori, I.C., Furuichi, T., Munemasa, S., Toyooka, K., Matsuoka, K., Murata, Y.,
574 Yamamoto, Y. (2010) Closing Plant Stomata Requires a Homolog of an Aluminum-Activated
575 Malate Transporter. *Plant Cell Physiol.* 10.1093/pcp/pcq016.

576 Sasaki, T., Ariyoshi, M., Yamamoto, Y., Mori, I.C. (2022) Functional roles of ALMT-type anion
577 channels in malate-induced stomatal closure in tomato and Arabidopsis. *Plant Cell Environ.*
578 10.1111/pce.14373.

579 Schroeder, J.I., Allen, G.J., Hugouvieux, V., Kwak, J.M., Waner, D. (2001) GUARD CELL
580 SIGNAL TRANSDUCTION. *Annu. Rev. Plant Physiol. Plant Mol. Biol.*
581 10.1146/annurev.arplant.52.1.627

582 Schwartz, A. (1985) Role of Ca^{2+} and EGTA on Stomatal Movements in *Commelina communis*
583 L.. *Plant Physiol.* 10.1104/pp.79.4.1003.

584 Shen, J.-L., Li, C.-L., Wang, M., He, L.-L., Lin, M.-Y., Chen, D.-H., Zhang, W. (2017)
585 Mitochondrial pyruvate carrier 1 mediates abscisic acid-regulated stomatal closure and the
586 drought response by affecting cellular pyruvate content in *Arabidopsis thaliana*. *BMC Plant*
587 *Biol*. 10.1186/s12870-017-1175-3.

588 Sweetman, C., Deluc, L.G., Cramer, G.R., Ford, C.M., Soole, K.L. (2009) Regulation of malate
589 metabolism in grape berry and other developing fruits. *Phytochemistry*
590 10.1016/j.phytochem.2009.08.006.

591 Trauelsen, M., Ulven, E.R., Hjorth, S.A., Brvar, M., Monaco, C., Frimurer, T.M., Schwartz,
592 T.W. (2017) Receptor structure-based discovery of non-metabolite agonists for the succinate
593 receptor GPR91. *Mol. Metab*. 10.1016/j.molmet.2017.09.005.

594 Trauelsen, M., Hiron, T.K., Lin, D., Petersen, J.E., Breton, B., Husted, A.S., Hjorth, S.A., Inoue,
595 A., Frimurer, T.M., Bouvier, M., et al. (2021) Extracellular succinate hyperpolarizes M2

macrophages through SUCNR1/GPR91-mediated Gq signaling. *Cell Rep*. 10.1016/j.celrep.2021.109246.

Urano, K., Maruyama, K., Ogata, Y., Morishita, Y., Takeda, M., Sakurai, N., Suzuki, H., Saito, K., Shibata, D., Kobayashi, M., et al. (2009) Characterization of the ABA-regulated global responses to dehydration in Arabidopsis by metabolomics. *Plant J.* 10.1111/j.1365-313X.2008.03748.x

Vahisalu, T., Kollist, H., Wang, Y.-F., Nishimura, N., Chan, W.-Y., Valerio, G., Lamminmäki, A., Brosché, M., Moldau, H., Desikan, R., et al. (2008) SLAC1 is required for plant guard cell S-type anion channel function in stomatal signalling. *Nature* 10.1038/nature06608.

Van Kirk, C.A., Raschke, K. (1978) Release of malate from epidermal strips during stomatal closure. *Plant Physiol.* 10.1104/pp.61.3.474.

Wada, H., Shackel, K.A., Matthews, M.A. (2008) Fruit ripening in *Vitis vinifera*: apoplastic solute accumulation accounts for pre-veraison turgor loss in berries. *Planta* 10.1007/s00425-008-0707-3.

Wang, X.-Q., Ullah, H., Jones, A.M., Assmann, S.M. (2001) G Protein Regulation of Ion Channels and Abscisic Acid Signaling in *Arabidopsis* Guard Cells. *Science* 10.1126/science.1059046.

Wang, Y.-F., Munemasa, S., Nishimura, N., Ren, H.-M., Robert, N., Han, M., Puzõrjova, I., Kollist, H., Lee, S., Mori, I., et al. (2013) Identification of Cyclic GMP-Activated Nonselective Ca^{2+}-Permeable Cation Channels and Associated *CNGC5* and *CNGC6* Genes in Arabidopsis Guard Cells. *Plant Physiol.* 10.1104/pp.113.225045.

Ye, W., Munemasa, S., Shinya, T., Wu, W., Ma, T., Lu, J., Kinoshita, T., Kaku, H., Shibuya, N., Murata, Y. (2020) Stomatal immunity against fungal invasion comprises not only chitin-induced stomatal closure but also chitosan-induced guard cell death. *Proc. Natl. Acad. Sci. USA.* 10.1073/pnas.1922319117.

Yu, Y., Chakravorty, D., Assmann, S.M. (2018) The G Protein β-Subunit, AGB1, Interacts with

622 FERONIA in RALF1-Regulated Stomatal Movement. *Plant Physiol.* 10.1104/pp.17.01277.

623 Zhang, W., Jeon, B.W., Assmann, S.M. (2011) Heterotrimeric G-protein regulation of ROS
624 signalling and calcium currents in Arabidopsis guard cells. *J. Exp. Bot.* 10.1093/jxb/erq424.

625

626 **Figure legends**

627 **Figure 1. Metabolome analysis in grapevine leaves during dehydration treatment.**

628 **(A)** PCA score plot of metabolomic datasets colored by the time of dehydration stress as clusters.
629 Dots represent biological replicates. Ellipse display 95% confidence regions of each cluster.

630 **(B)** Relative ABA levels. Fold changes were normalized to the values of 0 h. Data are the mean
631 ± SE.

632 **(C)** Volcano plot for the differential metabolites. Red and green dots mark the metabolites with
633 significantly increased and decreased level in 0 h versus 24 h, respectively. Upregulated
634 metabolites are defined VIP > 1, $\log_2$(Fold change) ≥ 1 and P-value > 0.05, downregulated
635 metabolites are defined VIP > 1, $\log_2$(Fold change) ≤ −1 and P-value > 0.05. P-value was
636 calculated by Welch's t-test.

637 **(D)** Categorization of the differential metabolites in **(C)**. Upper panel shows upregulated
638 metabolites and lower panel shows downregulated metabolites.

639 **(E)** Relative TCA cycle metabolite levels at different time points. Heat maps represent
640 $\log_2$(Fold change). Fold changes were normalized to the values of 0 h. Data were obtained from
641 three independent biological replicates. Abbreviations: F6P, fructose-6-phosphate; F1,6BP,
642 fructose 1,6-bisphosphate; GADP, glyceraldehyde 3-phosphate; 3PG, 3-phosphoglycerate; PEP,
643 phosphoenolpyruvate; Pyr, pyruvate; Cit, citrate; *cis*-Aco, *cis*-aconitate; Isocit, isocitrate; Keto,
644 α-ketoglutarate; Suc, succinate; Fum, fumarate; Mal, malate; Oxal, oxalate; Ser, serine; Trp,
645 tryptophan; Tyr, tyrosine; Phe, phenylalanine; Val, valine; Leu, leucine; Ile, isoleucine; Thr,
646 threonine; Asp, aspartate; Asn, asparagine; Met, methionine; Lys, lysine; Glu, glutamate; Gln,

647 glutamine; His, histidine; Pro, proline; Arg, arginine; GABA, γ-aminobutyrate.

648 **Figure 2. Ca^{2+} response to organic acids in guard cells.**

649 **(A and B)** Representative traces of fluorescence emission ratios (535/480 nm) in *A. thaliana*
650 guard cells expressing the Ca^{2+} sensor Yellow Cameleon 3.6. Grey bars indicate the time point
651 when treatment was applied. The guard cells were treated with organic acids 3 min after the
652 measurement.

653 **(C and D)** Percentage of number of guard cells showing different numbers of transient $[Ca^{2+}]_{cyt}$
654 increases. An increase in $[Ca^{2+}]_{cyt}$ is defined by an increase in fluorescence ratio by ≥0.1 U from
655 the baseline ratio. Data were obtained from Mock (25), Isocit (16) for **C**; Mock (51 guard cells),
656 Suc (31), Fum (28), Mal (44) Oxal (27), Keto (28), Cit (30), *cis*-Aco (29), Ace (33), Pyr (33),
657 Mal+La^{3+} (21) for **D**. Suc, succinate; Fum, fumarate; Mal, malate; Oxal, oxalate; Keto, α-
658 ketoglutarate; Cit, citrate; *cis*-Aco, *cis*-aconitate; Ace, acetate; Pyr, pyruvate; Isocit, isocitrate.
659 P-value was calculated by Fisher's exact test.

660 **Figure 3. SLAC1 activity in the presence of organic acids.**

661 **(A and B)** Representative whole-cell negative current recordings in Xenopus oocytes
662 expressing **(A)** VvSLAC1 or **(B)** AtSLAC1 in the presence of external organic acids. The
663 whole-cell negative current recording in the presence of external malate showed as red trace.
664 The voltage pulse was commanded to clamp the membrane potential from +60 mV to −120 mV
665 in ramp for 1.8 seconds with a holding potential of 0 mV.

666 **(C and D)** Average steady-state negative currents at −120 mV in Xenopus oocytes expressing
667 **(C)** VvSLAC1 or **(D)** AtSLAC1. Data were obtained from six oocytes per condition. Data are
668 the mean ± SE. Different letters indicate statistical significances within condition based on one-
669 way ANOVA with Tukey's HSD test, $P < 0.05$.

670 **Figure 4. Malate-induced stomatal closure is mediated by anion channels and Ca^{2+}.**

671 **(A and B)** Effects of organic acids on stomatal aperture in **(A)** *V. vinifera* or **(B)** *A. thaliana*
672 leaves. Male means maleate.

673 **(C–F)** Effects of inhibitors on malate-induced stomatal closure in **(C and D)** *V. vinifera* or **(E**
674 **and F)** *A. thaliana* leaves. Averages of stomatal apertures from four independent experiments
675 (n = 4) are shown. Data are the mean ± SE. Different letters indicate statistical significances
676 based on one-way ANOVA with Tukey's HSD test, $P < 0.05$.

677 **Figure 5. Malate signaling is mediated by cADPR, cAMP and IP_3.**

678 **(A–C)** Effects of inhibitors on malate-induced stomatal closure in **(A and C)** *A. thaliana* or **(B)**
679 *V. vinifera* leaves. Averages of stomatal apertures from four independent experiments (n = 4)
680 are shown. Data are the mean ± SE. Different letters indicate statistical significances based on
681 one-way ANOVA with Tukey's HSD test, $P < 0.05$.

682 **(D)** Representative traces of fluorescence emission ratios (535/480 nm) in *A. thaliana* guard
683 cells expressing the Ca^{2+} sensor Yellow Cameleon 3.6. Grey bar indicates the time point when
684 treatment was applied. The guard cells were treated with organic acids 3 min after the
685 measurement. Inhibitors were added 5 min before starting imaging.

686 **(E)** Percentage of number of guard cells showing different numbers of transient $[Ca^{2+}]_{cyt}$
687 increases. An increase in $[Ca^{2+}]_{cyt}$ is defined by an increase in fluorescence ratio by ≥0.1 U from
688 the baseline ratio. Data were obtained from Mock (10 guard cells), Mal (12), +Nicotinamide
689 (13), +Alloxan (10), +Neomycin (15), +SHAM (12). P-value was calculated by Fisher's exact
690 test.

691 **Figure 6. Malate signaling is mediated by G-proteins.**

692 **(A and B)** Effects of inhibitors on malate-induced stomatal closure in **(A)** *V. vinifera* or **(B)** *A.*
693 *thaliana* leaves.

694 **(C)** Effects of malate on stomatal aperture in *gpa1* and *agb1* mutants. Averages of stomatal
695 apertures from four independent experiments (n = 4) are shown. Data are the mean ± SE.
696 Different letters indicate statistical significances based on one-way ANOVA with Tukey's HSD
697 test, $P < 0.05$.

698 **(D)** Effects of GDPβS on malate-induced ROS production in *A. thaliana* guard cells. The ROS-

699 sensitive dye, 2',7'-dichlorodihydrofluorescein diacetate (H_2DCF-DA) was used for ROS
700 detection in guard cells. Fluorescence intensity was normalized to control values. Averages
701 from three independent experiments (n = 3) are shown. Data are the mean ± SE. Different letters
702 indicate statistical significances based on one-way ANOVA with Tukey's HSD test, $P < 0.05$.

703 **(E)** A proposed working model for malate-induced stomatal closure. The external signal of
704 malate is transmitted by G-proteins, which modulate the generation of second messengers,
705 including cAMP, cADPR and IP_3. This cascade leads to increases in $[Ca^{2+}]_{cyt}$, resulting in the
706 phosphorylation of SLAC1 by CDPKs. Additionally, G-proteins simultaneously modulate ROS
707 production, which contributes to SLAC1 phosphorylation. Extracellular malate directly
708 promotes anion transport through phosphorylated SLAC1, leading to a decrease in turgor
709 pressure and subsequent stomatal closure.

710 **Supplemental Figure 1. Metabolome analysis in grapevine leaves during dehydration**
711 **treatment.**
712 **Supplemental Figure 2. Ca^{2+} response to acetate in guard cells.**
713 **Supplemental Figure 3. The ion channel activity of VvSALC1 mutants.**
714 **Supplemental Figure 4. Malate-induced stomatal closure in other plant species.**
715 **Supplemental Figure 5. Malate-induced stomatal closure in the presence of inhibitors.**
716 **Supplemental Figure 6. ROS production in the presence of organic acids.**
717 **Supplemental Table 1. List of inhibitors used in this work.**
718 **Supplemental Table 2. List of primers used in this work.**
719 **Supplemental Data 1. Data table of metabolome analysis.**

Figure 1. Metabolome analysis in grapevine leaves during dehydration treatment.

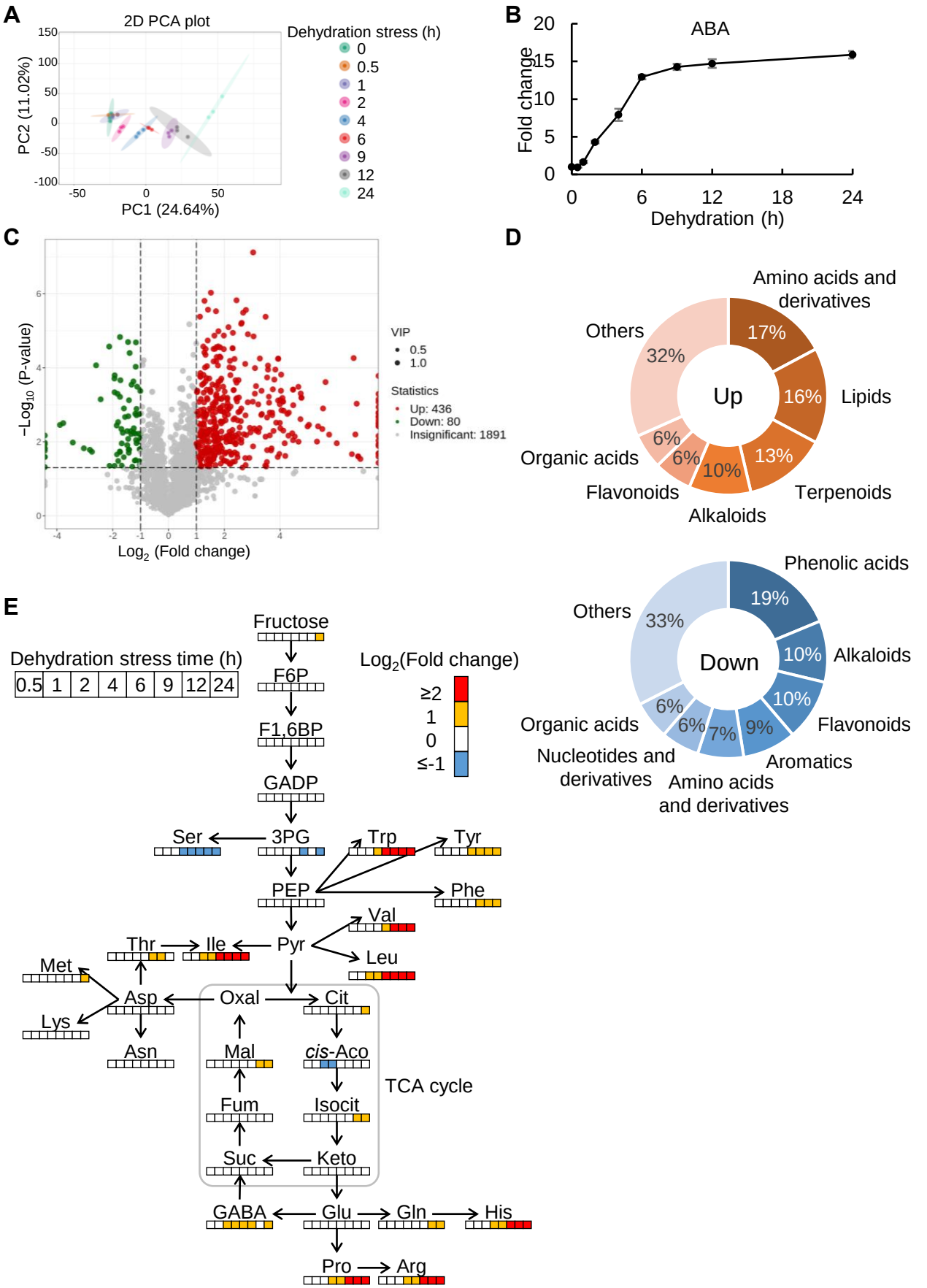

Figure 2. Ca^{2+} response to organic acids in guard cells.

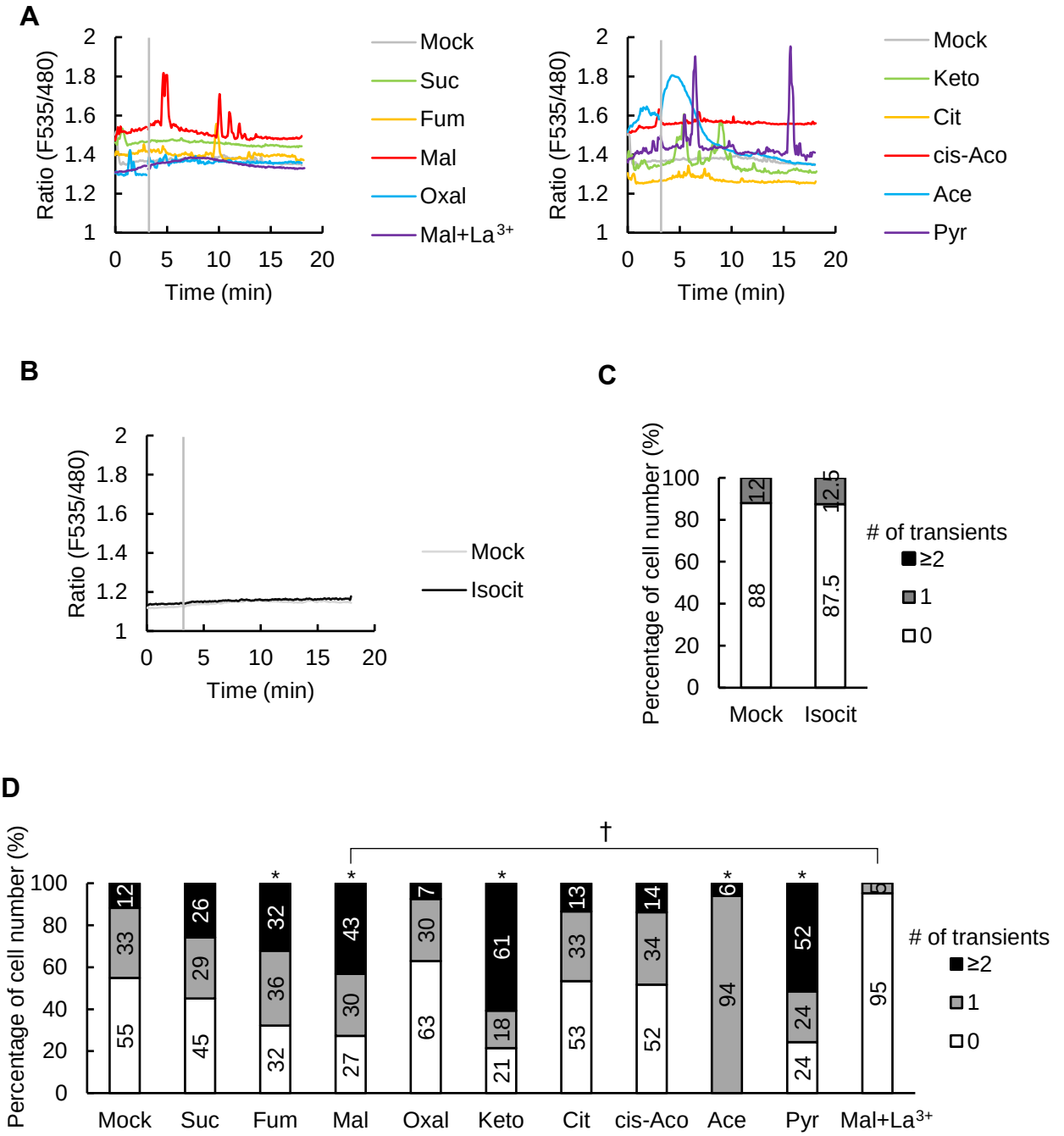

Figure 3. SLAC1 activity in the presense of organic acids.

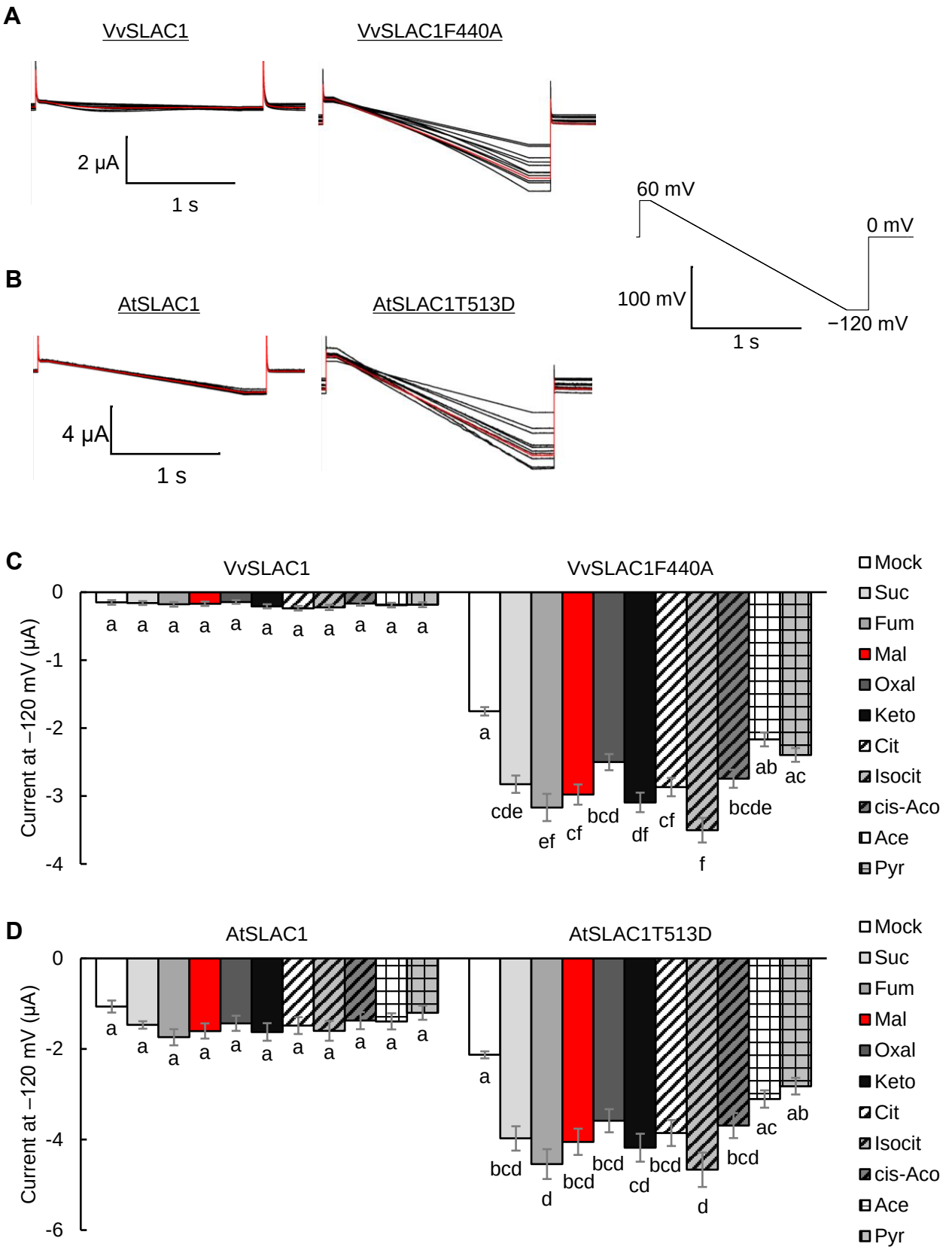

Figure 4. Malate-induced stomatal closure is mediated by anion channels and Ca^{2+} .

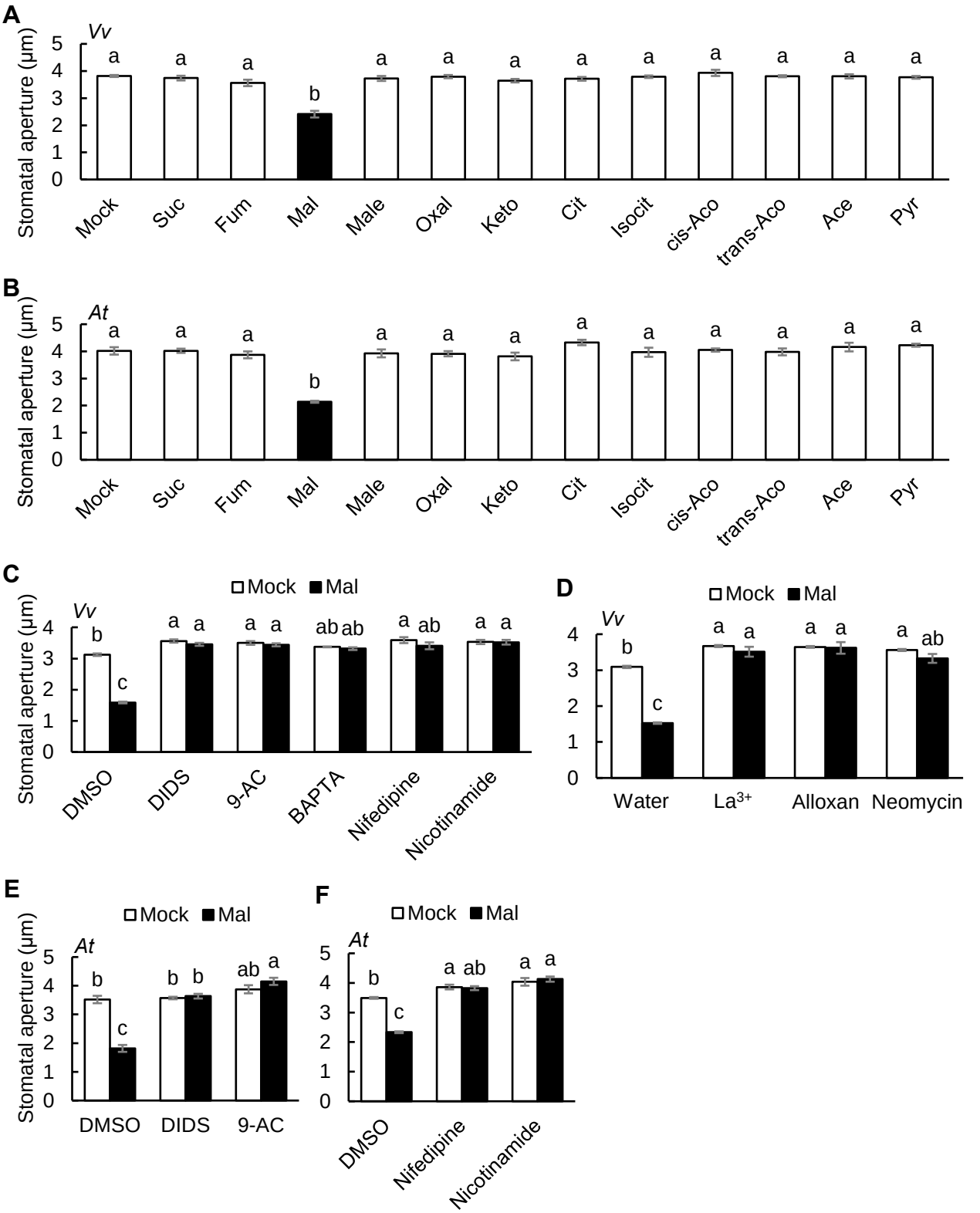

Figure 5. Malate signaling is mediated by cADPR, cAMP and IP_3.

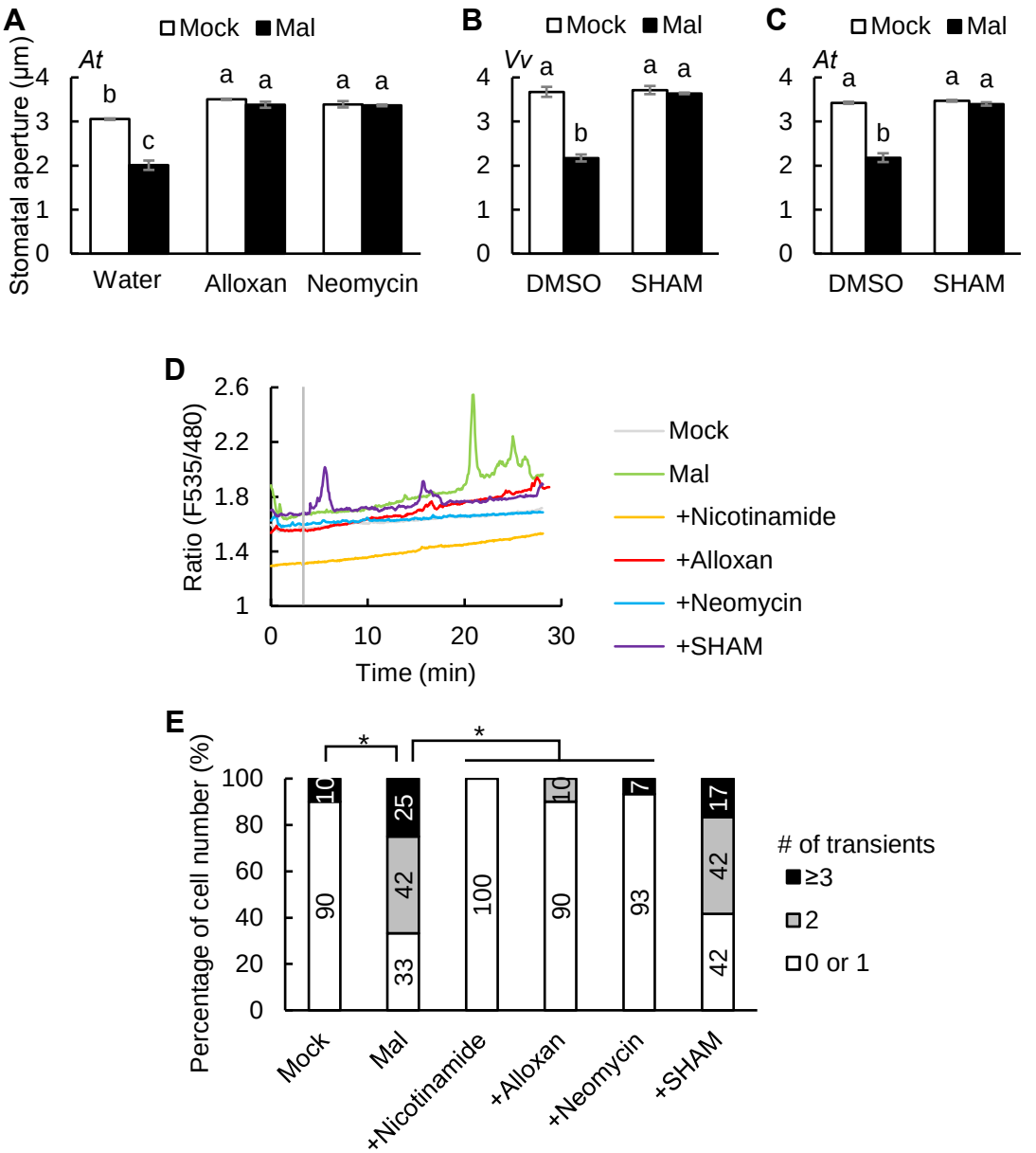
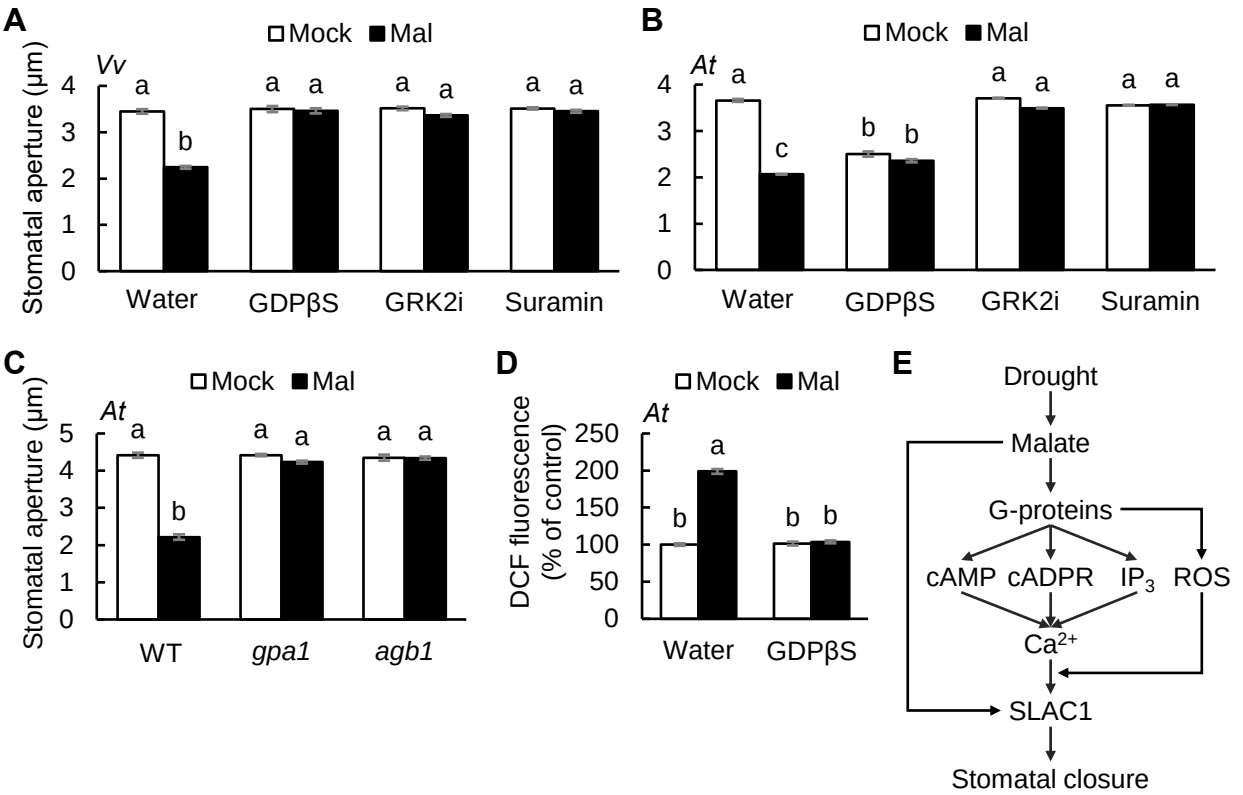
Figure 6. Malate signaling is mediated by on G-proteins.